Miniaturized Magnetic Sensors for Implantable Magnetomyography

Siming Zuo, Hadi Heidari,* Dario Farina, and Kianoush Nazarpour*

Magnetism-based systems are widely utilized for sensing and imaging biological phenomena, for example, the activity of the brain and the heart. Magnetomyography (MMG) is the study of muscle function through the inquiry of the magnetic signal that a muscle generates when contracted. Within the last few decades, extensive effort has been invested to identify, characterize and quantify the magnetomyogram signals. However, it is still far from a miniaturized, sensitive, inexpensive and low-power MMG sensor. Herein, the state-of-the-art magnetic sensing technologies that have the potential to realize a low-profile implantable MMG sensor are described. The technical challenges associated with the detection of the MMG signals, including the magnetic field of the Earth and movement artifacts are also discussed. Then, the development of efficient magnetic technologies, which enable sensing pico-Tesla signals, is advocated to revitalize the MMG technique. To conclude, spintronic-based magnetoresistive sensing can be an appropriate technology for miniaturized wearable and implantable MMG systems.

1. Introduction

Magnetomyography is the measurement and study of the magnetic manifestation of muscle activity, first formally proposed in

S. Zuo, Dr. H. Heidari
Microelectronics Lab (meLAB)
James Watt School of Engineering
University of Glasgow
Glasgow G12 8QQ, UK
E-mail: Hadi.Heidari@glasgow.ac.uk
Prof. D. Farina
Department of Bioengineering
Imperial College London
London SW7 2AZ, UK
Dr. K. Nazarpour
School of Engineering
Newcastle University
Newcastle upon Tyne NE1 7RU, UK
E-mail: Kianoush.Nazarpour@newcastle.ac.uk
Dr. K. Nazarpour
Biosciences Institute
Newcastle University
Newcastle upon Tyne NE2 4HH, UK

The ORCID identification number(s) for the author(s) of this article can be found under https://doi.org/10.1002/admt.202000185.

1972.[1] Cohen and Gilver defined the magnetomyogram signal to be a recording of one component of the magnetic field vector versus time, where the magnetic field at the point of measurement is due to currents generated by skeletal muscle. The correspondence between the MMG method and its electrical counterpart, that is the electromyography (EMG) technique.[2] Both stems directly from the Maxwell–Ampère law, as illustrated in **Figure 1**a. However, the ease at which the EMG signal can be recorded and the similarity between the temporal and spectral characteristics of the MMG and EMG signals have encouraged the academic and clinical communities to utilize the EMG method almost exclusively. As such the progress of the MMG method has been rather slow. Biomagnetic signals are typically weak. They can be polluted by environmental magnetic noise readily. Hence, most biomagnetic sensing studies take place in magnetically shielded rooms. Over the past four decades, the fidelity, temporal, and spatial resolution of macroscopic and noninvasive detection of biomagnetic signals have progressed significantly. Examples include the magnetocardiography (MCG) and magnetoencephalography (MEG) methods, evidenced by a significant difference in the number of publications since the 1970s when compared to the MMG studies. We will investigate the reasons for this significant difference and explore whether the technical constraints of measuring the magnetic fields from skeletal muscles have led to such a stark difference.

Two key drivers for the development of the MMG method: 1) poor spatial resolution of the EMG signals when recorded noninvasively on the skin where state-of-the-art EMG measurements are even using needle recording probes, which is possible to accurately assess muscle activity but painful and limited to tiny areas with poor spatial sampling points; 2) poor biocompatibility of the implantable EMG sensors due to the metal-tissue interface. The MMG sensors have the potential to address both shortcomings concurrently because: 1) the size of magnetic field reduces significantly with the distance between the origin and the sensor, thereby with MMG spatial resolution is uplifted; and 2) the MMG sensors do not need electrical contacts to record, hence if fully packaged with biocompatible materials or polymers, they can improve long-term biocompatibility.

The MMG signals can become an important indicator in medical diagnosis, rehabilitation, health monitoring and robotics control (Figure 1b).[3] Recent advances in technology have paved the way to remotely and continuously record and diagnosis
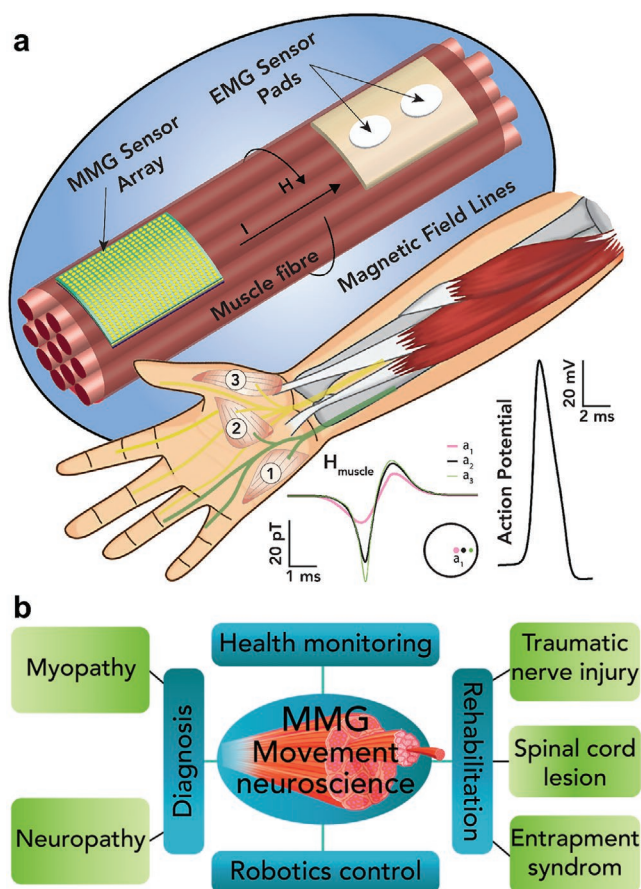
Figure 1. a) Schematic of the magnetic versus electric approaches to sensing muscle activity with the typical hand muscle locations: 1) M. abductor digiti; 2) Several intrinsic muscles of the thumb; 3) M. abductor pollicis; b) Potential application of MMG for diagnosis and rehabilitation of movement disorder, health monitoring and robotics control.

Hadi Heidari is a lecturer in the School of Engineering at the University of Glasgow, UK. He is leading the Microelectronics Laboratory and his research includes developing magnetoelectronics for neurotechnology devices. He is a member of the IEEE Circuits and Systems Society Board of Governors (2018–2020), IEEE Sensors Council Member-at-Large (2020-2021), senior member of IEEE and Fellow of Higher Education Academy (FHEA). He is the General Chair of the 27th IEEE ICECS 2020, and serves on the organizing committee of several conferences.

Dario Farina has been Full Professor at Aalborg University, Aalborg, Denmark, (until 2010) and at the University Medical Center Göttingen, Georg-August University, Germany, where he founded and directed the Institute of Neurorehabilitation Systems (2010–2016) until he moved to Imperial College London as a Chair in Neurorehabilitation Engineering. His research focuses on biomedical signal processing, neurorehabilitation technology, and neural control of movement. He has been the president of the International Society of Electrophysiology and Kinesiology (ISEK) (2012–2014).

Kianoush Nazarpour received his B.Sc. degree from K. N. Toosi University of Technology, Iran, in 2003, M.Sc. from Tarbiat Modarres University, Iran, in 2005, and Ph.D. from Cardiff University, UK, in 2008, all in electrical and electronic engineering. From 2007 to 2012, he held two postdoctoral researcher posts at Birmingham and Newcastle Universities. In 2012, he joined Touch Bionics, Inc., UK, as a senior algorithm engineer working on intelligent control of multifunctional myoelectric prostheses. Currently, he is a reader in biomedical engineering at Newcastle University. His research interests include intelligent sensing and biomedical signal processing and their applications in assistive technology.

individuals' disease of the muscle and the peripheral nerve.[4,5] Motivated by exploring the electrophysiological behavior of the uterus prior to childbirth, MMG was used mainly on health monitoring during pregnancy.[6–8] In addition, the MMG has the potential to be used in the rehabilitation such as the traumatic nerve injury, spinal cord lesion, and entrapment syndrome.[9–12]

However, compared with the magnitude of EMG signals in the scale of milli-volts, the MMG signal is extremely small and just in the range of pico (10^{-12}) to femto (10^{-15}) Tesla,[12] decreasing with the distance between the measurement point and the skeletal muscle. **Figure 2** illustrates the progress pathway of the biomagnetic sensors from SQUIDs,[1] atom magnetometer,[13,14] OPMs,[10,15] thin-film solid-state magnetic sensors,[16] to spintronic devices.[17,18] In a seminal work of Cohen and Gilver in 1972, they discovered and recorded MMG signals using superconducting quantum interference devices (SQUIDs). They led the development of MMG until now since it is the most sensitive device at moment with the femto-Tesla limit of detection (LOD), and possibly achieve atto-Tesla LOD with averaging.[19] The state-of-the-art MMG measurement is dominated by SQUIDs.[20] Nonetheless, their ultra-high cost and cumbersome weight limit the spread of this magnetic

ADVANCED
SCIENCE NEWS
www.advancedsciencenews.com

ADVANCED
MATERIALS
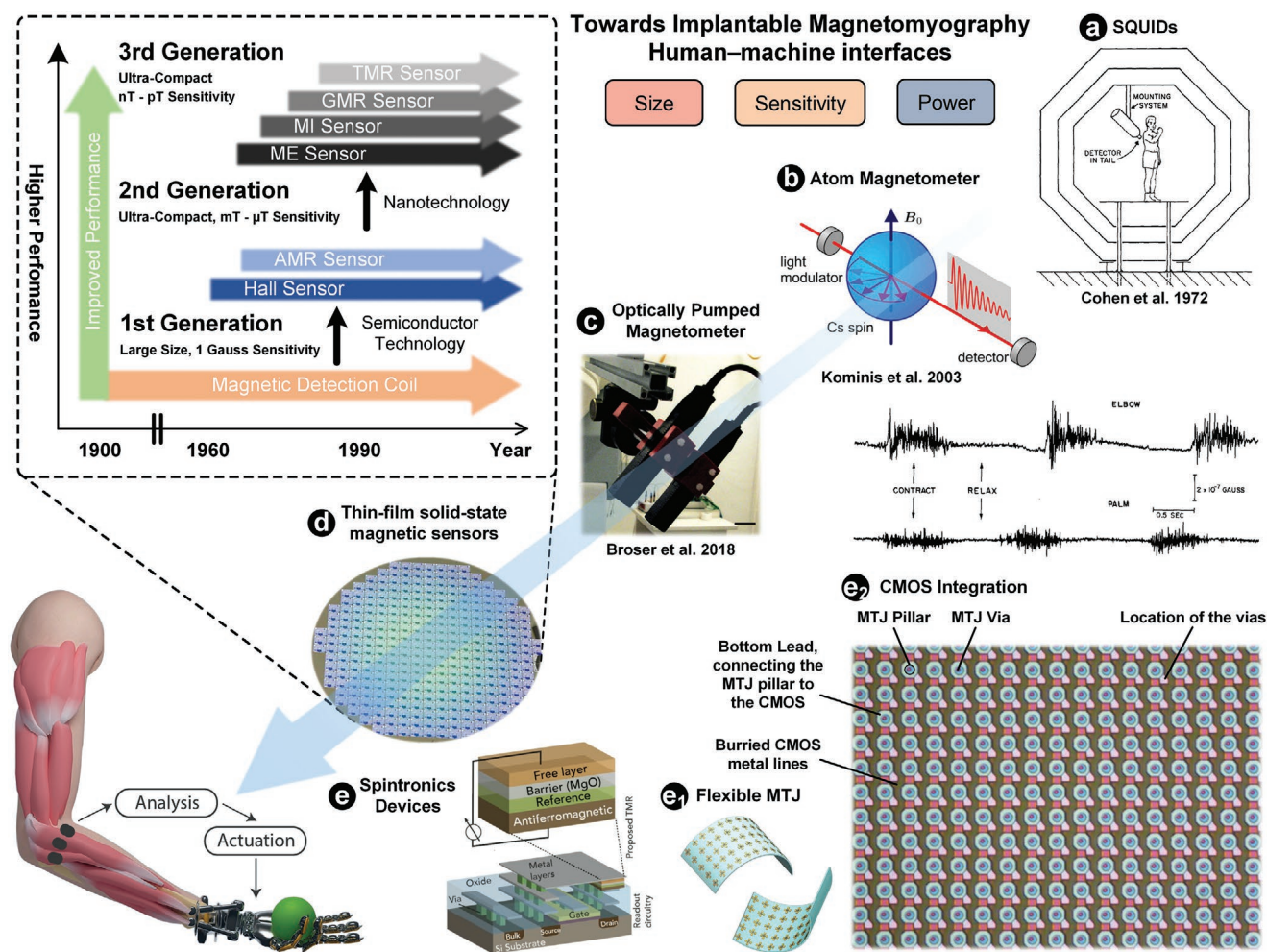TECHNOLOGIES
www.advmattechnol.de

Figure 2. A graphical overview of weak biomagnetic detection in skeletal muscle using MMG. The figure shows the miniaturization pathway from bulky SQUIDs to spintronic nanoscale devices. a) SQUIDs; Reproduced with permission.[1] Copyright 1972, Elsevier, b) Atom magnetometer; Reproduced with permission.[13] Copyright 2013, American Physical Society, c) Optical pumped magnetometer; Reproduced with permission.[10] Copyright 2016, Springer Nature, d) Thin-film solid-sate magnetic sensors; Reproduced with permission.[17] Copyright 2016, IEEE. Generations of miniaturization in detail, and e) spintronics devices,[16–18] from (e₁) flexible MTJ; Reproduced with permission.[107] Copyright 2017, Springer Nature to (e₂) standard CMOS technology; Reproduced with permission.[17] Copyright 2016, IEEE.

sensing technique. In the last several years, optically pumped magnetometers (OPMs) have been rapidly developed to study the innervation of the hand nerves and muscles as proof-of-concept investigations.[10,21,22] The MMG has not been a common method yet mainly due to its small magnitude, which can be easily affected by the magnetic noise in surrounding. For instance, the amplitude of the Earth magnetic field is about five million times larger and environmental noise from power lines can reach a level of nano-Tesla. Additionally, current experiments based on SQUIDs and OPMs for MMG sensing are conducted in heavily-shielded rooms, which are expensive and bulky for personal daily use. Consequently, the development of miniaturized, low-cost and room temperature biomagnetic sensing methods would constitute an important step toward the wider appreciation of biomagnetism.[23,24]

Nowadays, the integrated magnetic sensing technology has attracted interest as evidenced by a growing number of applications. For their adoption, it is critical to enhancing the micro-dimensional detection sensitivity and the functional robustness

of the sensors as required in real-time sensing and processing applications. The era of spin-based sensors began with the invention of the giant magnetoresistive (GMR) effect which concerns the intrinsic spin of the electron and its associated magnetic moment, instead of its fundamental electric charge.[25] The magnetoresistive effect is observed in artificial thin-film materials composed of alternate ferromagnetic and nonmagnetic layers.[26] In principle, spintronic sensors can accommodate compact sensors with sizes comparable to or smaller than that of the conventional SQUIDs for MMG. Yet, there are significant performance trade-offs in adopting this technology, particularly in terms of signal-to-noise ratio (SNR). Over the last decade, significant work has been performed to improve the detection range of spintronic sensors to pico-Tesla/$\sqrt{Hz}$ levels, for instance by utilizing the tunneling magnetoresistive (TMR) sensors.[27]

We intend to provide a perspective of miniature magnetic sensors for biomagnetic signal detection and argue for the feasibility of integrated TMR sensors for MMG applications. Firstly, the magnetic field generated by a typical skeletal muscle

**ADVANCED
SCIENCE NEWS**
www.advancedsciencenews.com

**ADVANCED
MATERIALS
TECHNOLOGIES**
www.advmattechnol.de

is modeled to provide a context in terms of the size of the MMG signals. Then, we study the state-of-the-art in pico-Tesla magnetic sensing technologies to provide guidance for the future development of an integrated MMG technology. In addition, we present simulation and experimental data supporting the view that integrated CMOS-compatible magnetoresistive sensors can be utilized for MMG sensing. We then discuss several technical challenges related to the biomagnetic sensing such as nulling the magnetic field of the Earth and movement artifacts. Finally, we posit that addressing these technical challenges and development of novel MMG sensing methods can facilitate a scientific revolution by providing additional details about the mechanics of the skeletal muscles. In addition, they can feature a breakthrough in human-machine interfacing applications such as control of prosthetic limbs.[28]

2. MMG Signals Modeling

The magnitude of the MMG signal depends upon several parameters. For instance, the distance between the source of the signal and the sensor can change the magnitude from nano-Tesla, when the MMG signals are recorded in isolated muscle fibers or implanted sensor below the skin, to pico-Tesla, when sensors are placed on the skin, outside of the body.[1,29–31] In the following, with **Figure 3**, we show the effect of the distance between the sensor and a single fiber to investigate the effect of the position of the muscle fiber bundles and radial and axial conductivities of the muscle fibers on the magnitude of the MMG signals.

The magnetic field produced by an action potential that travels in a single muscle fiber can be calculated using the approach developed by Roth and Wikswo in 1985.[32] Their method presents the advantage of using the Ampere's law, which allows disentangling the contributions to the magnetic field due to the currents present in each region of the system including the fibers, the bundle, the sheath of connective tissue and the bath. We use this model in the case of a muscle composed of several fibers. The geometry of the muscle is depicted in Figure 3a and a large set of parameters describing the muscle bundle are listed in **Table 1**.[33,34] From finite-element method (FEM) simulation results in 3D (Figure 3b) and 2D (Figure 3c), it shows that the total ring magnetic field is the superposition of each muscle fiber where nano to pico-Tesla range fields will be generated. The red arrows and color legend shows the direction and magnitude of magnetic fields respectively.

The muscle fiber was modeled as a cylindrical cable composed of 1200 compartments of 10 μm length and 50 μm diameter. A cylindrical fiber of diameter $a = 50$ μm was placed at a distance t from the center of the bundle. The bundle had a diameter $b = 150$ μm and 50 μm diameter fibers separated by an 10 μm interstitial space and were surrounded by a sheath with thickness $\delta = 10$ μm. All simulations were performed with NEURON (Hines and Carnevale 1997) and MATLAB (MathWorks 2017a).[35] The full expressions of calculation and boundary conditions are detailed by Roth and Wikswo 1985 and were solved using standard Python routines for a system of linear scalar equations.[32] Here, the parameters were adjusted to characterize the different currents to reproduce the action potential shape recorded on the soleus skeletal muscle cells
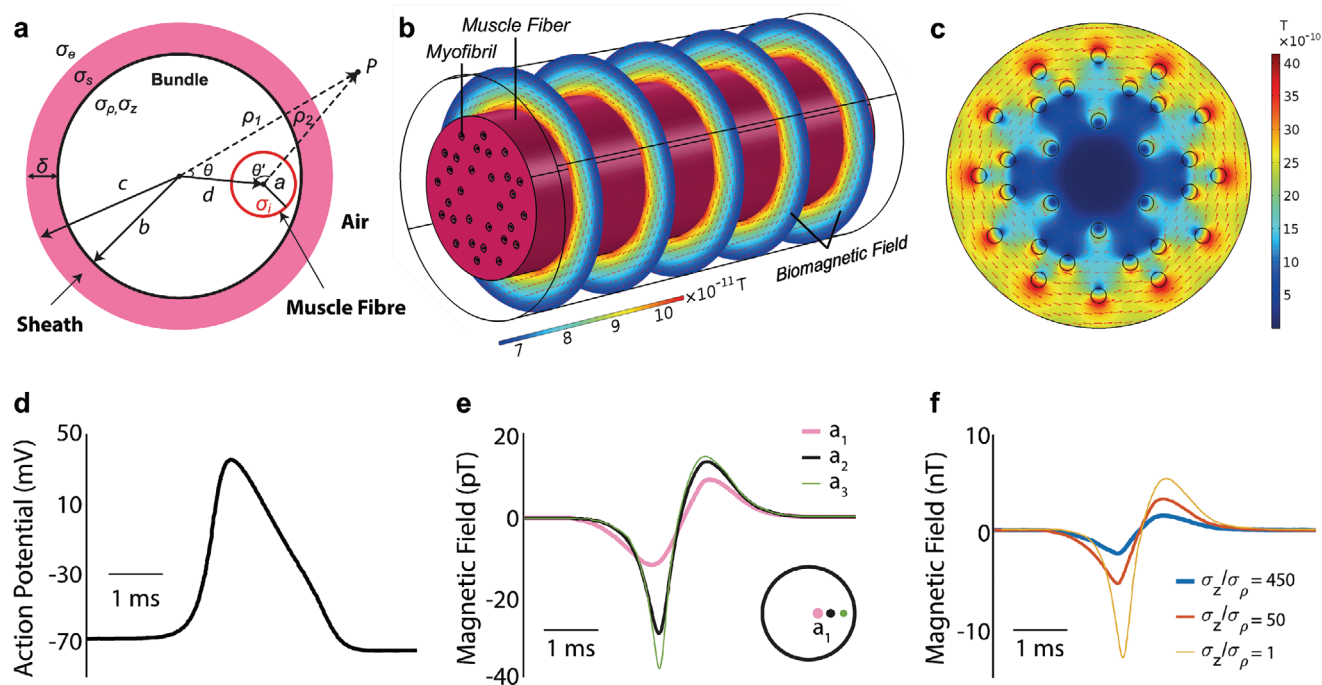

Figure 3. a) A scheme of the muscle model;[33] b) COMSOL 3D finite-element simulation results of biomagnetic fields generated from the muscle fiber; c) 2D results with muscle fiber and myofibrils; d) An action potential of the skeletal muscle fiber; e) Net magnetic field of a single fiber depending on its position inside the bundle. This net field contains different magnetic field components due to the currents flowing in the fiber B_i), the bundle B_b), the sheath B_s) and the saline B_e); f) Magnetic field generated by the entire muscle at 30 μm from the surface for different values of the ratio σ_z/σ_ρ ($\sigma_z = 5$ Ω^{-1} m^{-1}), where the axial and radial conductivities are σ_z and σ_ρ.[33,34]

ADVANCED
SCIENCE NEWS
www.advancedsciencenews.com

ADVANCED
MATERIALS
TECHNOLOGIES
www.advmattechnol.de

Table 1. Parameters to describe the muscle bundle.[33,34]

Parameter	Description	Value
a	fiber radius	4.00×10^{-5} m
b	radius of the muscle bundle	1.50×10^{-4} m
c	radius of the muscle bundle including the sheath	1.60×10^{-4} m
d	distance of the fiber from the center of the muscle bundle	8.00×10^{-5} m
ρ_1/ρ_2	field-point radius from the center of the muscle bundle	–
θ/θ'	orientation of the field point from the center of the muscle bundle	–
δ	thickness of the sheath around the muscle bundle	1.00×10^{-5}m
U	conduction velocity of the action potential	3.00 ms^{-1}
σ_i	internal conductivity of the axon in the muscle bundle	0.88 Ω^{-1}m^{-1}
σ_s	conductivity of the sheath around the muscle bundle	2.00 Ω^{-1}m^{-1}
σ_z	axial conductivity of the muscle bundle	5.00 Ω^{-1}m^{-1}
σ_ρ	radial conductivity of the muscle bundle	variable

under floating electrode recording conditions. Using this model and the transmembrane potential, as shown in Figure 3c, the x, y and z components of the magnetic action field at an observation point P, outside the muscle bundle, were calculated. As shown in Figure 3d, the net magnetic field was calculated for a single fiber located at distances d from the center of the bundle. We studied the behavior of the magnetic field due to the different currents as a function of axial and radial conductivities of the muscle bundle, that is σ_z and σ_ρ, respectively. As the ratio σ_z/σ_ρ increases, the shielding effect is more prominent, and hence the magnitude of the magnetic signal is decreased. In other words, when a fiber is close to the center

of the bundle, the current in the bundle shield generates the magnetic field. Finally, Figure 3e shows the total magnetic field B_{total} modeled at a point P, and the relative contributions due to the intracellular current B_i, the currents flowing in the bundle B_b, in the sheath B_s and in the external saline B_e. It should be noted that contributions from saline and sheath currents are much smaller than that of bundle currents. As such, extracellular bundle currents can be considered as the primary source of shielding.[1,29–31] In summary, the MMG signals can change from nano-Tesla, when recorded in isolated muscle fibers or implanted sensor below the skin, to pico-Tesla, when sensors are placed on the skin, outside of the body.

3. MMG Sensing Technologies

Magnetic sensors convert the magnetic field into measurable quantities such as voltages and current. **Figure 4** offers a broad overview of various environmental and biological magnetic signals and the currently available magnetic sensing technologies.[3] Most MMG signals are lower compared to other biological tissues like hearts and brains. The minimum spectral density could reach hundreds of fT/√Hz at low frequencies especially between 10 and 100 Hz.

In general, there are two categories of biomagnetic sensors. Those that are 1) sensitive only to the strength of the magnetic field, including devices such as OPM and atomic magnetometer that measure the magnitude of the magnetic field in the femto-Tesla range;[15,36,37] 2) sensitive to the strength and direction of the magnetic field, including SQUIDs,[38] Hall sensors,[39] magnetoresistive,[40] -electric,[41] and -impedance sensors,[42] conventional superconducting coils,[16] and fluxgates.[43] These vectorial sensors integrate multiple single-component sensors, which are placed on linearly independent directions. Some integrated vector magnetometer designs use micromachined electromechanical systems technology to obtain linear independence. In addition, some designs use in-plane Hall sensors
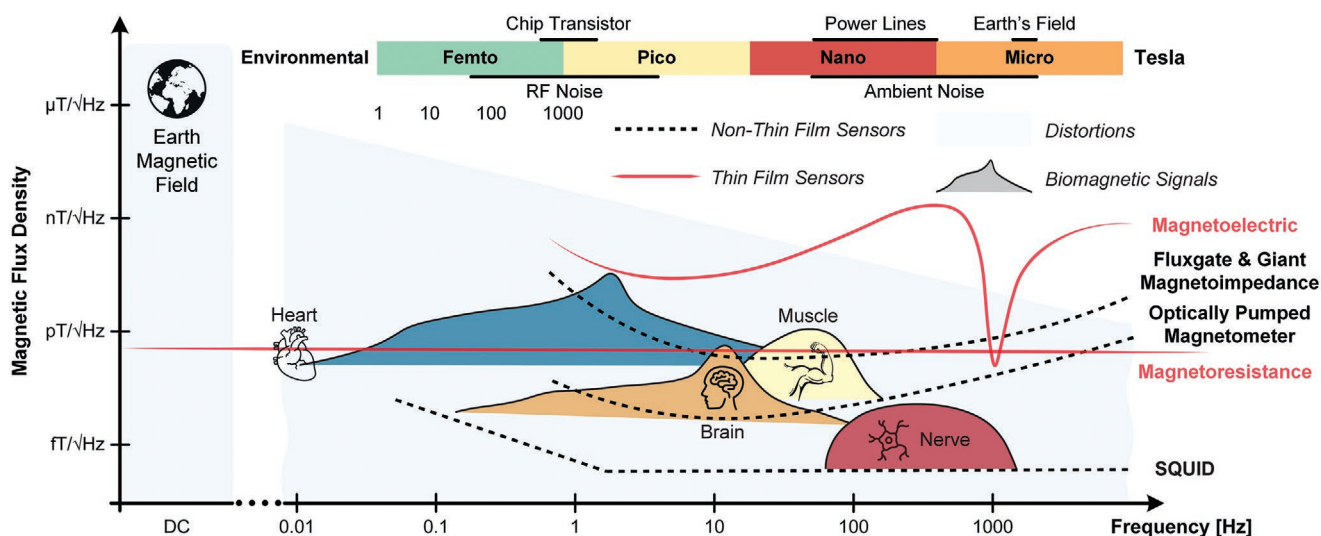

Figure 4. A summary of the strength of various example magnetic signals in comparison to biological signals and the existing magnetic sensing technologies.

**ADVANCED
SCIENCE NEWS**
www.advancedsciencenews.com

**ADVANCED
MATERIALS
TECHNOLOGIES**
www.advmattechnol.de

Table 2. A comparison of the magnetic sensing technologies for biosensing applications ($\sqrt{}$: Excellent, $\bullet$: Acceptable, $\blacktriangle$: Marginally acceptable, $\times$: unacceptable).

Principle	Sensitivity	Enhanced spatial resolution	Frequency	Miniaturization	Portability	Cost
OPM	$\bullet$	$\bullet$	DC	$\times$	$\times$	$\blacktriangle$
GMI	$\blacktriangle$	$\bullet$	DC-10 kHz	$\sqrt{}$	$\sqrt{}$	$\sqrt{}$
ME	$\bullet$	$\bullet$	DC-1 kHz	$\bullet$	$\sqrt{}$	$\sqrt{}$
Coils	$\bullet$	$\sqrt{}$	AC	$\times$	$\bullet$	$\sqrt{}$
Fluxgate	$\bullet$	$\sqrt{}$	DC-5 kHz	$\sqrt{}$	$\sqrt{}$	$\bullet$
SQUID	$\sqrt{}$	$\bullet$	DC-100 kHz	$\times$	$\times$	$\times$
MR	$\bullet$	$\sqrt{}$	DC-GHz	$\sqrt{}$	$\sqrt{}$	$\sqrt{}$

and instrumentation amplifiers to obtain all components of the magnetic field.[44]

A second broad categorization of magnetic sensors considers whether the magnetic field causes electrons to move through various layers of semiconductor material within the sensor, the so-called magneto-transport effect. Examples of technologies that benefit from the magneto-transport phenomenon include Hall probes and magneto-resistive, -electric and -impedance sensors. We compare the magneto-transport devices with the conventional SQUIDs, fluxgate sensors and the recently developed OPMs in **Table 2**.

Currently, SQUIDs are the most sensitive device with femto-Tesla sensing accuracy, and possibly achieve atto-Tesla (10^{-18} T) detection with averaging. The SQUIDs are widely used in many applications including in biomedical engineering for sensing MCG and MEG signals. Such sensitivity levels of SQUIDs require them to remain in a magnetically shielded room that is equipped with an appropriate cooling system for operation at liquid-helium temperature 4.2 K,[38] which also increases the cost of SQUIDs to several thousands of dollars.

Another fast developing magnetic sensing technology is the OPM.[45] Recently, OPMs with small physical size have been improved their LODs significantly during recent years and successfully used for a portable MEG system.[46] As shown in **Figure 5**a,[45] the OPM sensors, which utilize a vapor of spin-polarized rubidium atoms, can evaluate the transmission of laser light to detect the local magnetic field. Handheld and easy-to-use OPM sensors have recently become commercially especially from competing manufacturers, e.g., QuSpin Inc., FieldLine Inc. and Twinleaf.[47] Development of such sensors with small profile enables fitment in wearable devices such as a helmet.[45] Benefiting from the quantum sensing technology, these devices can attain the same sensitivity level that cryo-cooled SQUIDs offer, but in room temperature. Their lowest LODs below 100 fT/$\sqrt{}$Hz have been achieved.[45,48] Very recently, and as a proof of principle, OPMs were used to measure the MMG signals of the hand muscles, that were evoked by electrical stimulation of the nerves in the arm.[10,21,22] Unfortunately, it is still rather complex for the sensor setup and has a disadvantage that makes it an expensive instrument to own and operate.

Fluxgate sensors and giant magnetoimpedance magnetometers (GMIs) are well-established sensor concepts and both have similar dimensions, frequency ranges and LODs at low pT/$\sqrt{}$Hz ranges.[42,49,50] They were proved effective in real-time biomagnetic vector field measurement at ambient temperature

and without a magnetic shield. Despite they are very small and can be placed closer to the object, the worse LOD compared to OPMs and SQUIDs make them not be good candidates for the MMG measurement. Additionally, with a limited dynamic range, the manufacturing of fluxgates is complex and hence they are very expensive to use.[43]

With the emergence of the technologies that utilize the magneto-transport phenomenon, the field of magnetic sensing has been revolutionized.[17,40] Sensors with multilayered structure offer a small footprint, the possibility of integration into complementary metal-oxide-semiconductor (CMOS).[17] Although the sensitivity of current magneto-transport sensors is still lower than bulky SQUIDs and rival the performance that OPMs offer, unlike SQUIDs, they do not require any special operating conditions in terms of temperature. As such they are rather inexpensive and low power.

Thin-film magnetoelectric (ME) sensors have increasingly drawn attention over the past decade due to their small dimensions and the possibility of integration with micro-electromechanical systems. They have been successfully performed for MEG and MCG measurements.[51,52] The ME sensors offer passive detection, high sensitivity, large effect enhancement at mechanical resonances, and large linear dynamic range. This type of sensors recently has achieved a high pT/$\sqrt{}$Hz LOD range at low frequencies.[53–55] However, due to their physical principle, they suffer a complex measurement setup. Firstly, a stable DC bias magnetic field is required to keep optimum performance. Secondly, the ME sensor is based on mechanical resonance (resonance frequencies are typically 10 to 100 kHz), while biomagnetic signals are from 10 to 300 Hz normally. Therefore, magnetic frequency conversion techniques with modulation coils are needed for low-frequency detection, bringing a complicated signal processing process.[56]

At the same time, magnetic sensors based on the thin-film magnetoresistive (MR) effect have been widely explored over the past years as an effective alternative pico-Tesla biosensing approach at room temperature.[27,57–60] Supplied with a current or voltage, they convert an external magnetic field directly to a resistance. These sensors use ferro- and nonmagnetic materials whose magnetization aligns with the external field to maximize their resistance dynamic range,[61] including anisotropic magnetoresistance (AMR), GMR, and TMR. Figure 5b shows their general geometry and structure.

The cost of a typical MR sensor is approximately a tenth of a SQUID. Besides, MR sensors can measure the field at room
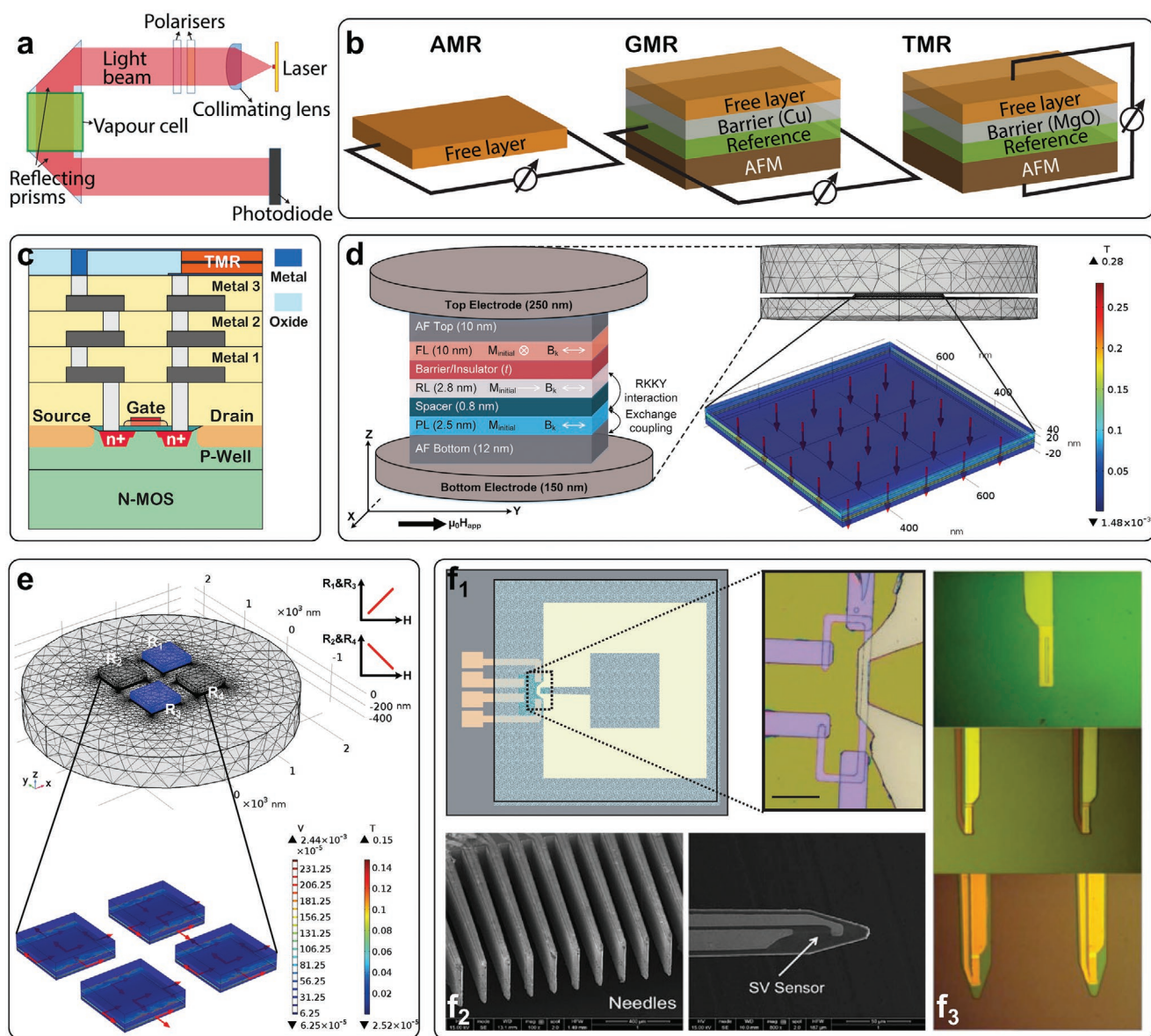
**ADVANCED
SCIENCE NEWS**

www.advancedsciencenews.com

**ADVANCED
MATERIALS
TECHNOLOGIES**

www.advmattechnol.de

Figure 5. State-of-the-art spintronic based biosensing sensors: a) A typical structure of an optically pumped magnetometer. Reproduced with permission.[45] Copyright 2017, Elsevier. b) The general geometry of MR sensors: AMR, GMR, and TMR; c) Monolithic Integration of the TMR sensor on standard CMOS. Reproduced with permission.[17] Copyright 2016, IEEE. d) Schematic of a state-of-the-art MTJ stack layout that was used for FEM simulations with the created mesh and the zoomed-in MTJ structure. Reproduced with permission.[83] Copyright 2018, IEEE, where the modeling result is an example achievable TMR response with fabricated sensors.[91,96] e) A typical Wheatstone bridge incorporating four TMR elements where two types of sensors with opposite dR/dH can offer robust sensing in the case of temperature drift. Reproduced with permission.[62] Copyright 2019, IEEE. f$_1$) Schematic view of a device, comprising a GMR sensor, measured with four probe contacts, with a superconducting loop of niobium, electrically isolated from the GMR by 400 nm of Si$_3$N$_4$, Reproduced with permission.[102] Copyright 2004, AAAS; f$_2$) SEM image an array with a spin valve (SV) sensor, Reproduced with permission.[66] Copyright 2013, Springer Nature; f$_3$) front-side view of the fabrication process for integrated TMR sensors in silicon microneedles, Reproduced with permission.[91] Copyright 2013, IEEE.

temperature without cooling. They have a wide dynamic range and are not affected by disturbance magnetic fields. Hence, they can operate with basic shielding. Furthermore, MR sensors have excellent temperature characteristics with Wheatstone Bridge structure that is the change in resistance due to fluctuations in temperature is negligible.[62]

The full compatibility between the novel spintronic sensors based on the MR effect and the conventional silicon technology

opens a realm of opportunities because MR sensors can be fabricated with high yields in sub-millimeter diameter substrates. These sensors can be integrated within standard CMOS chip together with the readout circuitry to ultimately achieve on-chip signal processing, amplification and noise cancellation.

The MR effect is the change in the resistance of a material under the influence of an external magnetic field. It was initially observed as a change in the resistance of Nickel and Iron

**ADVANCED
SCIENCE NEWS**

www.advancedsciencenews.com

**ADVANCED
MATERIALS
TECHNOLOGIES**

www.advmattechnol.de

according to the orientation of the applied magnetic field with respect to the direction of the current flow.[63] This effect was called the AMR, which arises from the spin-orbit coupling, reflecting the interaction between the spin of the conduction electrons and the crystal lattice.[63] Typical AMR values at room temperature are ≈5% for NiFe and CoFe bulk alloys and ≈2% for patterned thin films,[17] due to additional scattering caused by grain boundaries and other film interfaces. The low magnitude of the AMR effect, its intrinsic bulk properties to sense only the magnitude and not the direction and nonlinear output are the major drawbacks of AMR and encouraged the development of the GMR and TMR sensors.

Spin-based GMR sensors can realize reliable size-independent magnetic signal detection in the sub-nano-Tesla range at room temperature using micron-size structures. These features make GMR technology appropriate for enhanced biomagnetic source imaging.[17,18] The GMR effect is a fundamental phenomenon that occurs in magnetic materials ranging from nanoparticles over multilayered thin-films to permanent magnets. During the early stage, applications of GMR sensors had an industry-focus,[64] for information storage. In recent years, however, extensive research activity has been triggered to exploit the potentials of integrated GMR in ultralow biomagnetic signal detection.[65–73] Without increased cost or complicated structure, integrated GMR sensors bring aggregative performance improvements in the fabrication process, structure size, anti-noise ability, and sensitivity, taking advantages of multiple technologies and the inherent properties of GMR.[67,72,73]

The simplicity of the GMR mechanism is an excellent adventure for ultra-low biomagnetic signal detection. GMR sensors can detect pico-Tesla at the DC frequency magnetic field sensing at room temperature.[40] Thanks to the optimization of the thin-film materials, interfaces and electrical characteristics, the present form of GMR sensors in micro and nano dimensions is a mature technology with a substantial footprint in a wide range of applications.[74–76] This technology is a preferred choice for low magnetic fields detection with high spatial resolution. Recently, it has been utilized in the biomagnetic applications for MEG,[65] and MCG,[73] in which the sensitivity of the GMR sensors approaches that of the SQUIDs and paves the way for spintronic devices for functional biosensing and imaging. Smart GMR system can also be integrated with multiple components of Silicon-based circuits on small platforms such as lab-on-a-chip devices,[77,78] signal processing and communication modules. It will simplify the on-chip amplification and noise cancellation difficulty and reduce power consumption to sub-mW. Such miniaturized structures without sensitivity loss improve spatial resolution in weak fields sensing due to real-time and multi-mode process based on high compatibility with standard CMOS processes[72,79] The example of monolithic integration on standard CMOS with fabricated TMR sensor is shown in Figure 5c.[17] A recent study adopted biocompatible sensors based on GMR spintronics to simultaneously and locally record the magnetic fields from action potentials in a mouse muscle in vitro.[68] The GMR based micro-probes permitted the miniaturization and shaping required for in vivo/vitro magnetophysiology and represented a new fundamental tool to investigate the local sources of neuronal magnetic activities.[80]

Recent developments in physics and materials promise a new class of solid-state spintronic sensors based on the TMR effect, which occurs in magnetic tunnel junctions (MTJ).[81] These sensors can be faster, more reliable and of lower power than the existing spintronic sensors. The impact of the TMR sensors on the field of spintronics has been remarkable,[17] mainly due to the large magnitude of the observed magnetoresistances at room temperature that surpasses that of the AMR and GMR sensors. The TMR effect has been known since 1975,[82] and is observed on ferromagnetic (FM) spin tunneling junctions consisting of FM-insulator-FM layers. The basic structure of a TMR-based sensor is shown in Figure 5b. The magnetic orientation of the reference layer is fixed, whilst the magnetic orientation of the free layer will change in accordance with the direction of the external magnetic field. Classical physics predicts that there should be no current flowing through the insulating barrier when a voltage is applied to the FM electrodes on both sides of an MTJ. However, when the insulating barrier is ultrathin, in the scale of a few nanometers, a quantum tunneling effect may take place in the junction, which allows electrons to transfer from one FM layer to the other. An MTJ with a bias voltage may, therefore, exhibit electrical conducting properties and its electrical resistance varies as a function of the magnetic field strength over a certain field range.[83]

Because of their higher MR ratio and better SNR, TMR sensors have been gradually replacing the GMR devices. In addition, TMR sensors have a tunable response and adjustable operation range.[84] Therefore, they are ideal candidates for applications in which pico-Tesla level operation at room temperature, small footprint and cost are key factors. In addition, they are compatible with standard silicon integrated circuit technology,[85,86] allowing for large-scale fabrication and closed packed implementations, which is ideal for portable solutions.[87,88]

Still, it is difficult to predict how precisely a sensor behaves when an external magnetic field is applied, especially when the sensor structure comprises several layers of materials. Fabricating and testing all possible combinations will consume too much time and money. Instead, simulations can be utilized to model the behavior of certain material combinations and sensor shapes. For example, modeling of MTJ devices based on MgO barrier show higher MR ratio in comparison to the Al_2O_3 barrier devices.[17,89] We showed that such simulation results and parameters can be extracted and imported to the Cadence Spectre simulator for integration with a CMOS-based readout circuit.[39,90–94] We believe that this structure can offer a platform to develop ultra-sensitive, smart and compact sensors for MMG sensing. To reliably compile the TMR model in the Cadence environment, we adopted a FEM environment such as COMSOL Multiphysics.[83] The extracted data was then exported to Cadence using Verilog-A language so that the model can be designed and integrated into a standard CMOS-based analog front-end (AFE) circuit. This setting offered the possibility of including circuits for on-chip amplification, signal processing, and noise cancellation.

Recent work proposed FEM simulations of magnetic biosensors,[95] and evaluation of their performance in terms of the TMR ratio and linearization range.[83] Figure 5d shows an MTJ

**ADVANCED
SCIENCE NEWS**

www.advancedsciencenews.com

**ADVANCED
MATERIALS
TECHNOLOGIES**

www.advmattechnol.de

stack, which is a multilayer between two leads in a current-perpendicular-to-plane geometry with double-exchange electrodes, consisting of bottom antiferromagnet (AFM), reference layer, spacer, reference layer, barrier, sensing layer and top-AFM. The 3D structure of the MTJ can be divided into small elements with tetrahedral meshes of user-defined sizes. This FEM model was used to estimate the current distribution of the MTJ with different strength of the magnetic field.[83] The computational meshes with different resolutions to reduce discretization errors and an enlarged view of the thin film structure where the color legend shows magnetic flux density and the arrow represents the direction of the current density. In addition, in order to minimize undesired effects, such as the temperature drift in sensing, various circuit designs can be used. For instance, a typical Wheatstone bridge configuration to minimize the temperature drift was shown in Figure 5e.[62] Compared with achievable TMR responses with fabricated sensors,[91,96] state-of-the-art modeling results show a higher TMR ratio and better linearization.[83]

4. MMG with Spintronic Sensors

The optimization of materials and the fabrication process to obtain high MR ratio are challenging tasks.[59,90,97,98] The TMR sensors with the MgO barrier are highlighted as the most competitive sensors that could achieve pico-Tesla level detection at room temperature and low-frequency domain. Previous efforts have already demonstrated detection limits in the pico-Tesla/$\sqrt{Hz}$ range by coupling MR sensors with magnetic flux guides without a significant increase in the noise levels.[57,99,100] The TMR sensors with integrated magnetic flux guides improve the sensitivity of the sensor by amplifying locally the magnetic fields that reach the sensing layer.[101] The integrations of the MR sensors are demonstrated with state-of-the-art examples in Figure 5f.[17,66,102,91] The potential applications of TMR sensors are directly detecting magnetic signals generated from human organs. The full compatibility between the TMR technologies and the Silicon industry opened a new way of the system miniaturization. One of the important biosensing applications is achieved by the integration of an array of MR sensors on sharp, machined probes,[66,91] as shown in Figure 5f$_1$,f$_2$. They enjoy the ability to measure directly and locally the magnetic fields related to human activity such as brain and heart etc., at room temperature. The recent in vitro measurement for brain activity monitoring upon electrical stimulation is demonstrated in Figure 5f$_3$. It requires special sensor geometries where sharp probes incorporated single or large arrays of TMR sensors with microelectrodes microfabricated at the same fabrication process. Integrated state-of-the-art MgO-based TMR sensors into Si needles, it can be used as a miniature tool for the biomagnetic sensing at very weak fields level, especially pico to femto Tesla with a low-frequency domain. Currently, MultiDimension Technology has achieved the sensitivity of 100–300 mV V^{-1} Oe^{-1} in a larger prototype commercial TMR sensors, TMR9001/9002.[103] With continuous research pT level detection has been achieved at room temperature,[27,57–59,103,104] and fT detectivities have been reported at low temperature (77 K) by using superconductor magnetic flux concentrators.[69,71]

Moreover, the recent progress achieved the integration of functional MR sensors with flexible materials for new devices and applications.[105–108] As demonstrated in recent work,[105] the MR technology has pushed the integration limits toward stretchable substrates to form a flexible and bendable sensor solution. Motivated by the continued researches for wearable and implantable sensing, microfabricated devices on flexible substrates can bend and conform to the nonplanar geometries. For instance, the TMR sensors have been measured on polyimide substrates,[109] where the TMR sensor maintains its MR ratio when compared with rigid substrates such as Si or glass. The advantages of polyimide-based devices include flexibility, thermal stability, chemical resistance, high mechanical modulus, and biocompatibility.

Recently, we showed the first result of highly sensitive TMR-recorded ultralow MMG signals from the human hand muscle at room temperature. **Figure 6**a illustrates the experimental setup. To reduce noise sources such as the acoustic noise and disturbances of magnetic and electric fields from the earth and surrounding equipment, both sensor characteristics and MMG measurements were carried out in a shielded environment to counteract the influence of external magnetic fields. An active compensation technique is employed to the whole system, mainly consisting an active geomagnetic field cancellation box with an array of tri-axial square Helmholtz coils. The system is operated with the magnetic field compensation on three direction components (x, y, z) at the same time. Thus, the uniform reverse fields cancel each magnetic field component B_x, B_y, and B_z of the geomagnetic field respectively. Additionally, as shown in Figure 6b, stainless steel tubes are also employed in the middle of the box to further shield the environmental magnetic field. Finally, the whole system is only with a residual magnetic field of 4 nT.

To minimize 1/f noise of the sensor,[110] 1102 TMR elements are connected in 58 series and 19 parallel, as illustrated in Figure 6c. The total chip size is 6 mm × 4 mm while each TMR sensor is 100 × 100 μm (Figure 6d). The TMR stack consists of (unit: nm) [5 Ta/25 CuN] × 6/5Ta/5 Ru/20 IrMn/2 CoFe30/0.85 Ru/2.6 CoFe$_{40}$B$_{20}$/1MgO/2 CoFe$_{40}$B$_{20}$/0.21 Ta/4 NiFe/0.20 Ru/6 IrMn/2 Ru/5 Ta/10 Ru. Figure 6e shows an entire stack structure by a transmission electron microscope. The bottom NiFe and CoFeB free layers show anti-ferromagnetic coupling where the magnetization reversal process reflects that of the thick NiFe layer.[16] Additionally, an annealing process was performed after micro-fabrication to ensure that orthogonal magnetic axes of the free and pinned layers were aligned.[96]

The miniaturized MMG system includes the Wheatstone bridge with four TMR sensors, as well as the digital and analog electronics parts which are needed for generating selected useful information from the measured MMG signals. A real-time readout system for newly-developed TMR sensors has been proposed and implemented. Figure 6a shows functional blocks of system architecture, which comprises sensors, analog front-end (AFE), and digital back-end signal processing units. First of all, the Wheatstone bridge can operate in the voltage-mode or the current-mode by using two toggle switches as selectors. The stable power supplies are provided by a voltage regulator and a current generator. The proposed AFE includes a transimpedance amplifier (TIA), an
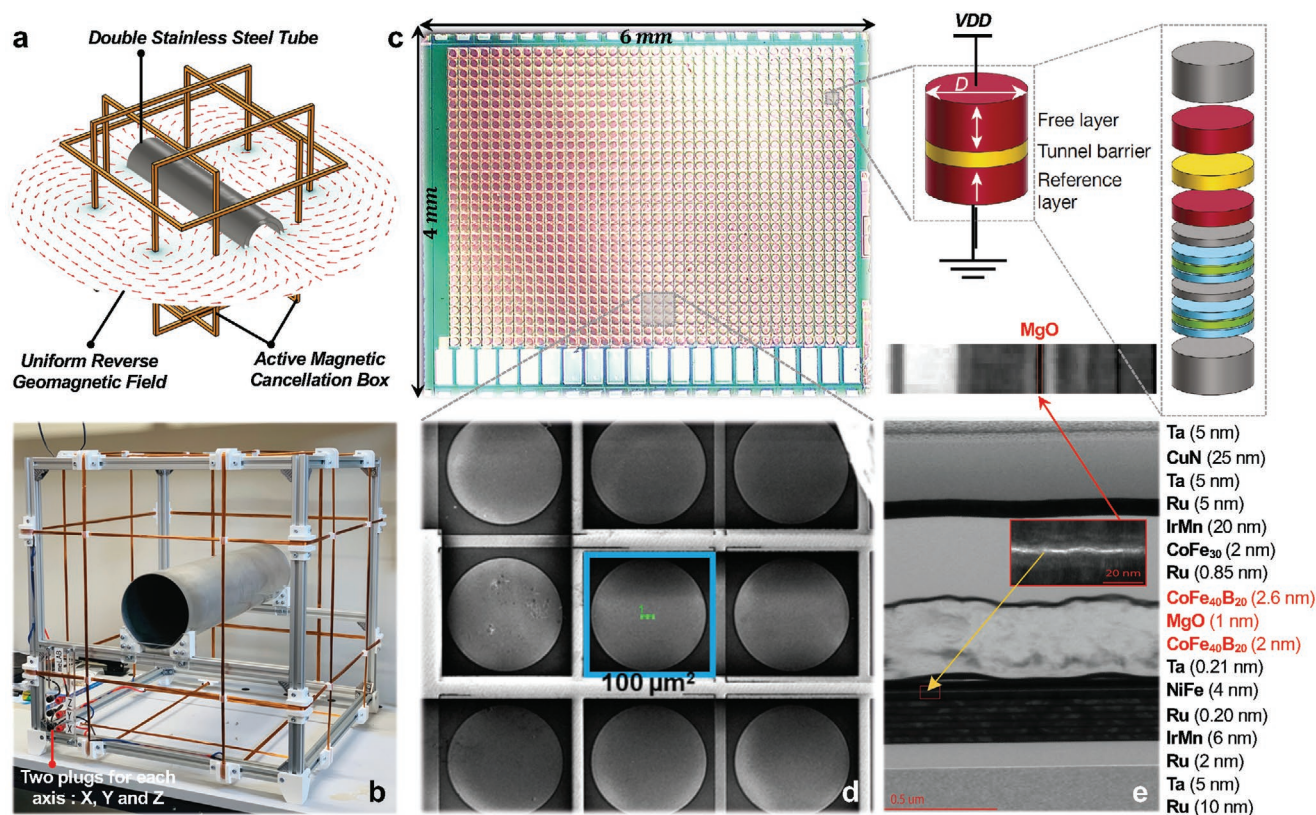
**ADVANCED
SCIENCE NEWS**
www.advancedsciencenews.com

**ADVANCED
MATERIALS
TECHNOLOGIES**
www.advmattechnol.de

Figure 6. a) Measurement setup with FEM simulations; b) A 3D-printed active geomagnetic field cancellation box with stainless steel tubes; c) A microscope image of TMR sensor array; d) Enlarged image with a size of 100 μm² per TMR element; e) Transmission electron microscope image of the entire stack structure where the red box shows indication of MgO barrier surrounded by Fe:Co matrix.

instrumentation amplifier, bandpass filters, a programmable gain amplifier, an analog multiplexer, micro control unit, which includes an analog-to-digital converter (ADC). Finally, the signals are transmitted through a wireless module and then extracted, classified and displayed in a LabVIEW interface on the laptop.

The AFE details are demonstrated in **Figure 7**b. Four TMR elements form a Wheatstone bridge in a parallel configuration to cancel the temperature drift.[111,112] The currents flowing through R_1 and R_3 are in the opposite direction to R_2 and R_4. This way, the magnetic field generated by the current flow is parallel or antiparallel to the reference layer, respectively, while the free magnetization layer will rotate with the field orientation. As a result, the sensor input current is applied to terminals a and b, while the output current is measured between terminals c and d and then sent to the AFE and the back-end signal processor. An ultralow noise amplifiers are utilized to amplify the differential signals with external noise filtering switched capacitors,[62] allowing the integration of TMR sensors on CMOS without decreasing the measurement resolution. A power management unit with low-dropout regulators (LDOs) provides all required power supply voltages from a single 12 V battery. In particular, the advantages of scaling and higher density integration must be balanced against the requirements of low noise design, uniform power density, and surface temperature distribution, better component matching, and immunity to parameter variations.[113] In addition, the spatial resolution can be improved by scaling an array of sensors that can measure the biomagnetic field from different points. To enhance the system immunity against external interferences, integrated circuits with ultralow noise current source for TMR biasing and low-noise variable gain amplifier are implemented.[67] Several detailed examples demonstrate the integration procedures of advanced TMR sensors.[75,92] Therefore, the MR sensing technologies based on the TMR effect makes it possible to detect weak MMG signals.

5. MMG Implementation and Discussion

5.1. Execution and Experimental Results

An example of a linearized sensor curve measured for MgO-based TMR device is presented in **Figure 8**a. With an original resistance of 2.295 kΩ, the linear range of the sensor is about from −1 to 1 Oe. The average $R \times A$ is 9 kΩ μm² and the TMR ratio is 152%. For the full bridge setup, the measured voltage change of each TMR element is 280 Ω μm² Oe⁻¹ and the sensitivity is measured as ≈0.617 V Oe⁻¹. The challenge is indeed to detect very weak fields (fT to nT), which usually have a low-frequency domain. Here, the $1/f$ noise is the dominant factor, as exemplified in Figure 8b with the noise spectra of an MTJ array. The estimated minimum field that this sensor can detect is ≈20 pT at 100 Hz.

**ADVANCED
SCIENCE NEWS**

www.advancedsciencenews.com

**ADVANCED
MATERIALS
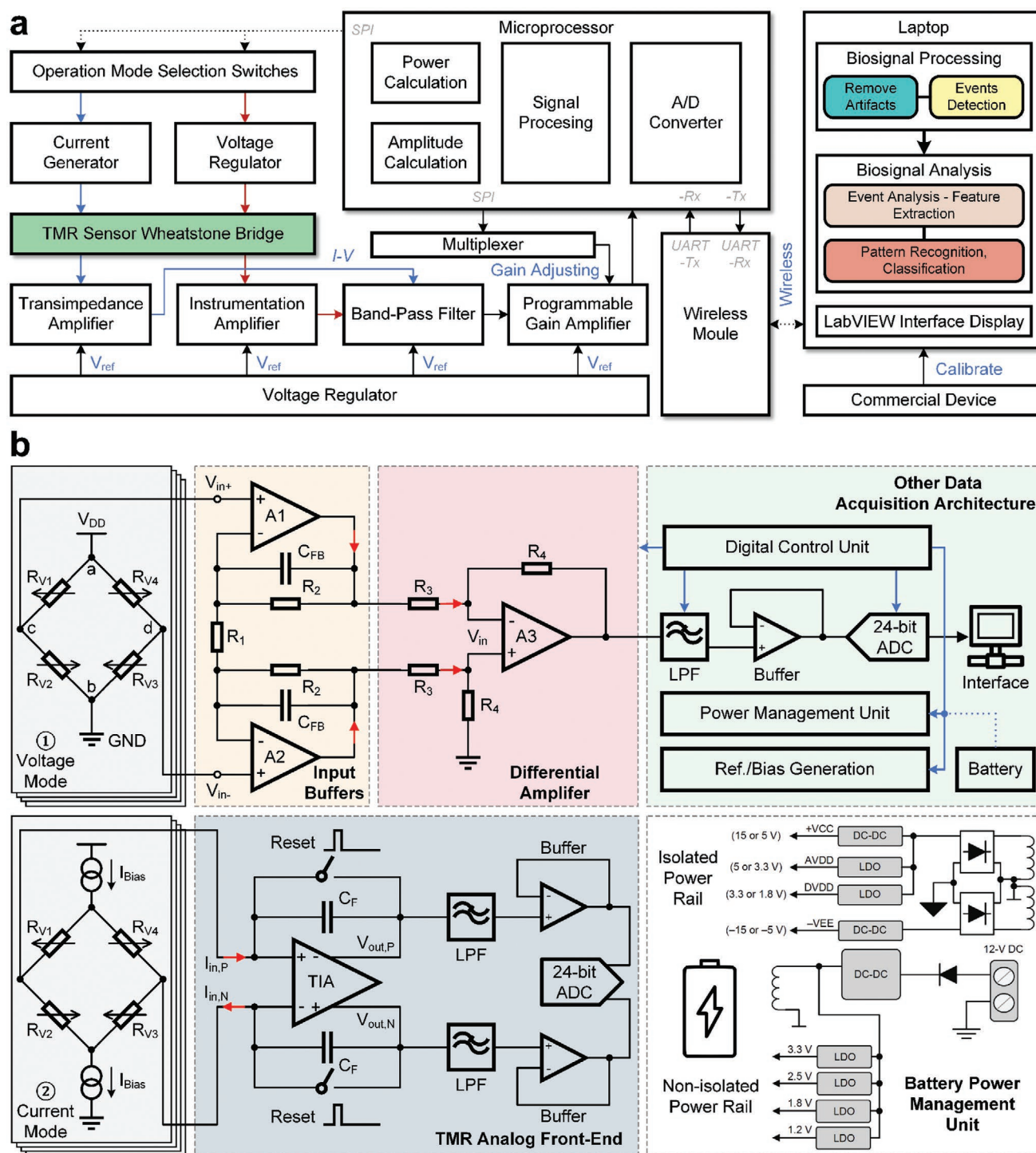TECHNOLOGIES**

www.advmattechnol.de

Figure 7. a) A block diagram of a general processing chain for TMR sensors that can be utilized for MMG applications. The signals are recorded by an array of sensors. Afterward digitally controlled analog processing can be performed, which in general improves the readout of the sensor signals. The measured signals are passed to a digital signal enhancement stage, before a detailed analysis can be performed; b) Overview of MMG signal detection with two different operations: 1) voltage-mode and 2) current-mode.

Placing the TMR sensor array exactly on the skin of abductor pollicis brevis hand muscle, the transverse component of the magnetic field can be measured. The surface EMG signals were recorded at the same time as an effective reference. The 100 s MMG signals from the proposed TMR system were recorded and analyzed to verify the whole process of muscle activities. Figure 8a shows a clear difference in time series between when the hand was tense and when
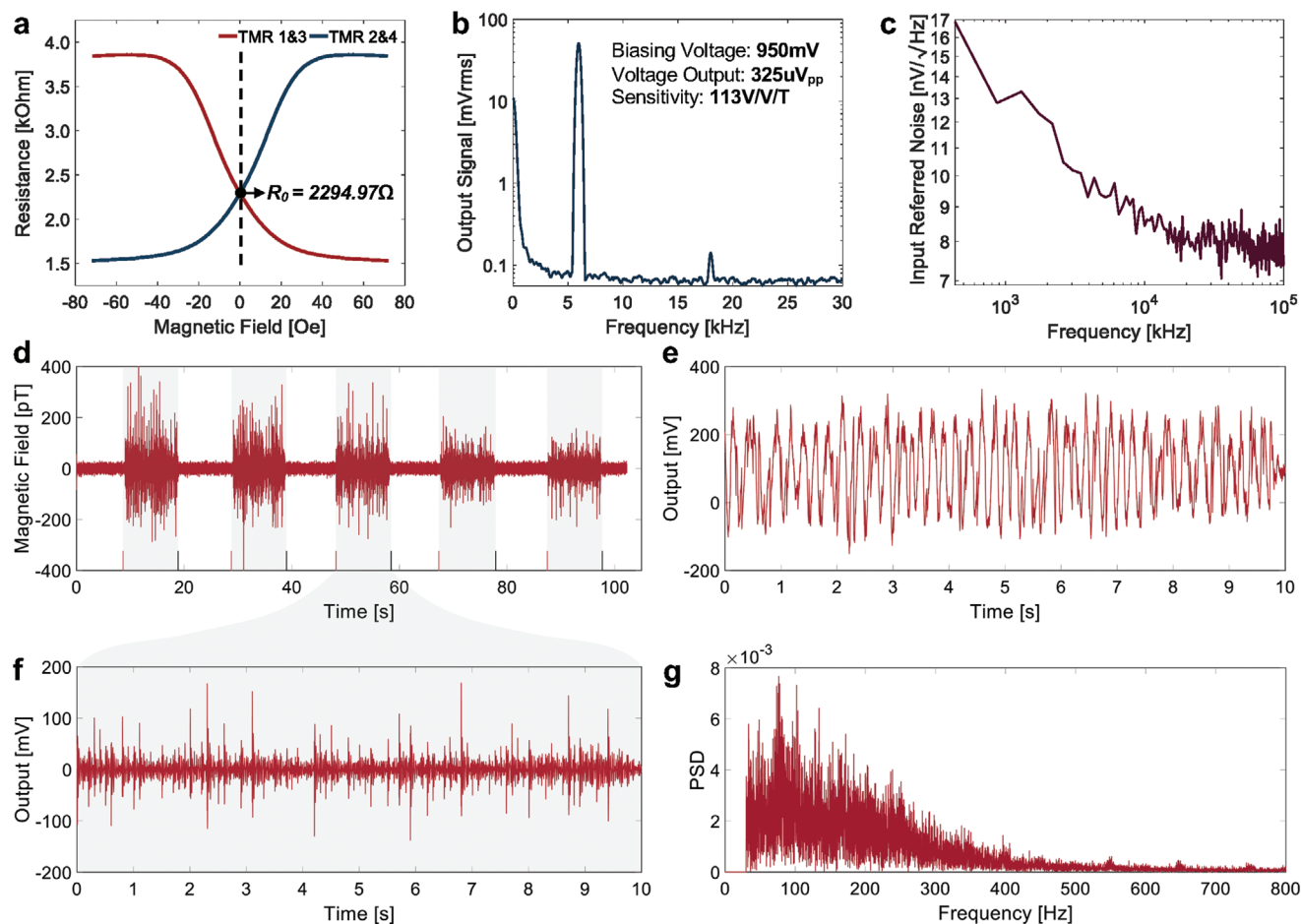
**ADVANCED
SCIENCE NEWS**

www.advancedsciencenews.com

**ADVANCED
MATERIALS
TECHNOLOGIES**

www.advmattechnol.de

Figure 8. a) Measured resistances variation of the TMR sensor with magnetic fields; b) Sensitivity measurement when applying a bias voltage of 950 mV; c) Noise measurement. The corner frequency is around 9 kHz; d) Measured MMG signals (100 s) from the proposed TMR system when the hand muscles were relaxed and tense respectively; e) Raw MMG signals without filtering when the hand muscles were in the tense state; f) MMG signals after a 20th-order bandpass (30 to 300 Hz) Butterworth filter; g) Power spectrum from the tense hand muscles.

the hand was relaxed. The first type is a time-domain with an amplitude of 200 pT, corresponding to periods when the hand is tense. This amplitude of the MMG signals corresponds to the accepted ideas about the magnetic field of skeletal muscles. The second type is a time-domain with an amplitude of 20 to 30 pT, corresponding to the lengths of time when the hand is relaxed. This amplitude is roughly equal to the amplitude of the noise activity records in a relaxed hand. Without filtering, the raw MMG signal from the tense muscles is illustrated in Figure 6b, which include wideband noise and movement artifacts. Nevertheless, by using the 20th-order bandpass Butterworth filter of 30–300 Hz (Figure 6c), the signals not only became clearer but also confirmed that the positions of the peaks for both the MMG and EMG were almost the same. The approximate amplitude of 200 pT was observed, which is consistent with the reported value measured by SQUIDs.[12] Finally, the MMG power spectrum is shown in Figure 6d with a wideband frequency range, in which the MMG signals of the tensed hand state is many times greater than noise. At frequencies from 30 to 300 Hz, the signal-to-noise ratio is greater than 20.

5.2. Discussion of Technical Challenges

Current approaches for MMG sensing are limited due to relatively low SNR. The magnitude of the EMG signal is on the scale of milli-volts and that for the MMG signal is on the scale of pico-Tesla,[114] depending upon different measurement conditions. The magnetic field of the Earth can reach values in the order of micro-Tesla and the typical magnetic environmental noise can be in the order of 100 nano-Tesla/√Hz. However, the magnetic fields that are generated by the skeletal muscle are significantly smaller. In addition, it should be highlighted that the sensor interference (thermal and $1/f$ noises) largely degrades the response linearity and low-frequency detection ability in the TMR sensors. Various approaches have been studied to boost the SNR, including electromagnetic shielding techniques, reference channels, and signal processing. Currently, there are no off-the-shelf solutions for the detection of MMG signals in nonmagnetically shielded environments at room temperature. Essentially, the uniform background magnetic fields from the Earth would lead to saturating the sensor.[115] Therefore, it would be a huge challenge to isolate

the extremely weak bio-magnetic components of the measured signals in the low-frequency domain (<500 Hz). A recent technique to null the background static magnetic field in MEG consists of a shield to attenuate background noise from micro-Tesla to nano-Tesla.[46] Then, a set of bi-planar electromagnetic coils generate nano-Tesla fields, equal and opposite to the remnant Earth's field, thereby cancelling it out. In addition, a proportional integral derivative (PID) algorithm was used to control the currents in the field-nulling coils. This allows the calculation of currents which generate fields that are equal and opposite to those measured by the reference array.

In the past, the measurements of the MMG signals were performed using SQUIDs with the detection limit of 3 fT/√Hz at a cooling environment. However, this technology is extremely expensive to both acquire and run and need specialized facilities such as a shielded room and a cooling system. Moreover, the SQUIDs detect the magnetic field at a short distance from the point of operation in the body. However, current human-machine interfacing concepts based on MMG rely greatly on the development of low-cost, flexible and miniaturized magnetic detectors. Flexible and miniaturized sensor structures show great potential to improve temporal and spatial resolutions since the signal magnitude will be greater with the reduced distance between sensor and muscle tissue.

The magnitude of the MMG signal varies with the third power of the distance between the transducer and the current source. As a result, significant dimensional changes of the skeletal muscle during contraction or a movement of the human or the body part under investigation can affect the MMG signal, which can be troublesome. Consequently, all the human studies in vivo collected the MMG signal while volunteers performed isometric contractions.[1,29,116] Therefore, in order to avoid the effects of movements as much as possible, implantable MMG sensors would be more appropriate for the human-machine interfacing, such as control of prosthetic limbs,[28] to reduce the effect of muscle movement.

6. Conclusion and Future Direction

We described potential approaches for the next generation recording of the MMG signals and discussed their benefits against conventional systems. The generation of the bio-magnetic field by skeletal muscles was reviewed, compared with EMG and discussed in terms of the physical and mathematical relationship. In addition, the final characteristic properties of the main magnetic sensors technologies for finding the optimal candidate of the MMG systems were provided. We advocated for the development of miniaturized magnetic sensors and the integration of MTJs into standard CMOS technology for MMG sensing. Then, we proposed several research strategies on how to fill the gap between the conventional and the next-generation MMG sensors that could achieve high-performance sensing. Moreover, we evaluated and discussed the challenges related to biomagnetic sensing such as nulling the magnetic field of the Earth. We provided a roadmap toward miniaturization of magnetic sensors for low-field biomagnetic detection.

Future development of MR-sensors will open new possibilities for the next generation of MMG systems. A significant effort would be needed to optimize the physical and functional properties of the MR sensors and to find suitable materials. From the signal processing perspective, advanced data analysis techniques are highly required for cancelling the noise and offset at the output of the sensors. We conclude that wearable and implantable MMG can soon become a promising and complementary approach for the measurement of muscle activity.

Conflict of Interest

The authors declare no conflict of interest.

[1] D. Cohen, E. Givler, *Appl. Phys. Lett.* **1972**, *21*, 114.

[2] S. J. Oh, *Clinical Electromyography: Nerve Conduction Studies*, Lippincott Williams & Wilkins, USA **2008**.

[3] J. Malmivuo, R. Plonsey, *Bioelectromagnetism: Principles and Applications of Bioelectric and Biomagnetic Fields*, Oxford University Press, USA **1995**.

[4] A. G. Filler, K. R. Maravilla, J. S. Tsuruda, *Neurol. Clin.* **2004**, *22*, 643.

[5] E. Yamabe, T. Nakamura, K. Oshio, Y. Kikuchi, H. Ikegami, Y. Toyama, *Radiology* **2008**, *247*, 409.

[6] H. Eswaran, H. Preissl, J. D. Wilson, P. Murphy, C. L. Lowery, *Am. J. Obstet. Gynecol.* **2004**, *190*, 1598.

[7] H. Eswaran, H. Preissl, P. Murphy, J. D. Wilson, C. L. Lowery, in *2005 IEEE Engineering in Medicine and Biology 27th Annual Conf.*, IEEE, Shanghai, China **2006**, pp. 6665–6667.

[8] H. Eswaran, R. B. Govindan, A. Furdea, P. Murphy, C. L. Lowery, H. T. Preissl, *Eur. J. Obstet. Gynecol. Reprod. Biol.* **2009**, *144*, S96.

[9] B.-M. Mackert, J. Mackert, G. Wübbeler, F. Armbrust, K.-D. Wolff, M. Burghoff, L. Trahms, G. Curio, *Neurosci. Lett.* **1999**, *262*, 163.

[10] P. J. Broser, S. Knappe, D.-S. Kajal, N. Noury, O. Alem, V. Shah, C. Braun, *IEEE Trans. Neural Syst. Rehabil. Eng.* **2018**, *26*, 2226.

[11] D. Escalona-Vargas, S. Oliphant, E. R. Siegel, H. Eswaran, *Neurourol. Urodyn.* **2019**, *38*, 151.

[12] M. A. C. Garcia, O. Baffa, *Front. Physiol.* **2015**, *6*, 228.

[13] Z. D. Grujić, P. A. Koss, G. Bison, A. Weis, *Eur. Phys. J. D* **2015**, *69*, 135.

[14] D. Sheng, S. Li, N. Dural, M. V Romalis, *Phys. Rev. Lett.* **2013**, *110*, 160802.

[15] Y. J. Kim, I. Savukov, *Sci. Rep.* **2016**, *6*, 24773.

**ADVANCED
SCIENCE NEWS**

www.advancedsciencenews.com

**ADVANCED
MATERIALS
TECHNOLOGIES**

www.advmattechnol.de

[16] P. Ripka, M. Janosek, *IEEE Sens. J.* **2010**, *10*, 1108.

[17] P. P. Freitas, R. Ferreira, S. Cardoso, *Proc. IEEE* **2016**, *104*, 1894.

[18] P. P. Freitas, F. A. Cardoso, V. C. Martins, S. A. M. Martins, J. Loureiro, J. Amaral, R. C. Chaves, S. Cardoso, L. P. Fonseca, A. M. Sebastião, *Lab Chip* **2012**, *12*, 546.

[19] R. L. Fagaly, *Rev. Sci. Instrum.* **2006**, *77*, 101101.

[20] M. N. Ustinin, S. D. Rykunov, M. A. Polikarpov, A. Y. Yurenya, S. P. Naurzakov, A. P. Grebenkin, V. Y. Panchenko, *Math. Biol. Bioinf.* **2018**, *13*, 480.

[21] G. Z. Iwata, Y. Hu, T. Sander, M. Muthuraman, V. C. Chirumamilla, S. Groppa, D. Budker, A. Wickenbrock, *arXiv Prepr. arXiv1909.11451* **2019**.

[22] E. Elzenheimer, H. Laufs, W. Schulte-Mattler, G. Schmidt, *IEEE Trans. Neural Syst. Rehabil. Eng.* **2020**.

[23] W. A. McClay, N. Yadav, Y. Ozbek, A. Haas, H. T. Attias, S. S. Nagarajan, *Brain Sci.* **2015**, *5*, 419.

[24] R. Fukuma, T. Yanagisawa, Y. Saitoh, K. Hosomi, H. Kishima, T. Shimizu, H. Sugata, H. Yokoi, M. Hirata, Y. Kamitani, *Sci. Rep.* **2016**, *6*, 21781.

[25] M. N. Baibich, J. M. Broto, A. Fert, F. N. Van Dau, F. Petroff, P. Etienne, G. Creuzet, A. Friederich, J. Chazelas, *Phys. Rev. Lett.* **1988**, *61*, 2472.

[26] S. A. Wolf, D. D. Awschalom, R. A. Buhrman, J. M. Daughton, S. Von Molnar, M. L. Roukes, A. Y. Chtchelkanova, D. M. Treger, *Science* **2001**, *294*, 1488.

[27] W. F. Egelhoff, P. W. T. Pong, J. Unguris, R. D. McMichael, E. R. Nowak, A. S. Edelstein, J. E. Burnette, G. A. Fischer, *Sens. Actuators, A* **2009**, *155*, 217.

[28] H. Heidari, S. Zuo, A. Krasoulis, K. Nazarpour, in *40th Int. Conf. IEEE Engineering in Medicine and Biological Society*, IEEE, Honolulu, HI, USA **2018**, pp. 2116–2119.

[29] T. Masuda, H. Endo, T. Takeda, *Clin. Neurophysiol.* **1999**, *110*, 384.

[30] R. S. Wijesinghe, *J. Electr. Electron.* **2014**, *3*, 1.

[31] F. Barbieri, V. Trauchessec, L. Caruso, J. Trejo-Rosillo, B. Telenczuk, E. Paul, T. Bal, A. Destexhe, C. Fermon, M. Pannetier-Lecoeur, *Sci. Rep.* **2016**, *6*, 39330.

[32] B. J. Roth, J. P. Wikswo, *Biophys. J.* **1985**, *48*, 93.

[33] N. Ganapathy, J. W. ClarkJr, O. B. Wilson, *Math. Biosci.* **1987**, *83*, 61.

[34] F. L. H. Gielen, B. J. Roth, J. P. Wikswo, *IEEE Trans. Biomed. Eng.* **1986**, *BME-33*, 910.

[35] M. L. Hines, N. T. Carnevale, *Neural Computation.* **1997**, *9*, 1179.

[36] I. K. Kominis, T. W. Kornack, J. C. Allred, M. V Romalis, *Nature* **2003**, *422*, 596.

[37] V. Shah, S. Knappe, P. D. D. Schwindt, J. Kitching, *Nat. Photonics* **2007**, *1*, 649.

[38] R. Körber, J.-H. Storm, H. Seton, J. P. Mäkelä, R. Paetau, L. Parkkonen, C. Pfeiffer, B. Riaz, J. F. Schneiderman, H. Dong, S. Hwang, L. You, B. Inglis, J. Clarke, M. A. Espy, R. J. Ilmoniemi, P. E. Magnelind, A. N. Matlashov, J. O. Nieminen, P. L. Volegov, K. C. J. Zevenhoven, N. Höfner, M. Burghoff, K. Enpuku, S. Y. Yang, J.-J. Chieh, J. Knuutila, P. Laine, J. Nenonen, *Supercond. Sci. Technol.* **2016**, *29*, 113001.

[39] H. Heidari, E. Bonizzoni, U. Gatti, F. Maloberti, *IEEE Trans. Circuits Syst.* **2015**, *62*, 1270.

[40] P. P. Freitas, R. Ferreira, S. Cardoso, F. Cardoso, *J. Phys.: Condens. Matter* **2007**, *19*, 165221.

[41] G. Srinivasan, *Annu. Rev. Mater. Res.* **2010**, *40*, 153.

[42] T. Uchiyama, K. Mohri, Y. Honkura, L. V. Panina, *IEEE Trans. Magn.* **2012**, *48*, 3833.

[43] P. Ripka, *Sens. Actuators, A* **2003**, *106*, 8.

[44] C. S. Roumenin, D. I. Nikolov, *Electron. Lett.* **2003**, *39*, 1646.

[45] E. Boto, S. S. Meyer, V. Shah, O. Alem, S. Knappe, P. Kruger, T. M. Fromhold, M. Lim, P. M. Glover, P. G. Morris, *NeuroImage* **2017**, *149*, 404.

[46] E. Boto, N. Holmes, J. Leggett, G. Roberts, V. Shah, S. S. Meyer, L. D. Muñoz, K. J. Mullinger, T. M. Tierney, S. Bestmann, *Nature* **2018**, *555*, 657.

[47] I. Savukov, Y. J. Kim, V. Shah, M. G. Boshier, *Meas. Sci. Technol.* **2017**, *28*, 035104.

[48] O. Alem, T. H. Sander, R. Mhaskar, J. LeBlanc, H. Eswaran, U. Steinhoff, Y. Okada, J. Kitching, L. Trahms, S. Knappe, *Phys. Med. Biol.* **2015**, *60*, 4797.

[49] H. Karo, I. Sasada, *J. Appl. Phys.* **2015**, *117*, 17B322.

[50] S. Nakayama, T. Uchiyama, *Sci. Rep.* **2015**, *5*, 1.

[51] R. Jahns, R. Knochel, H. Greve, E. Woltermann, E. Lage, E. Quandt, *IEEE Int. Symp. on Medical Measurements and Application Proc.*, IEEE, Bari, Italy **2011**.

[52] V. Röbisch, S. Salzer, N. O. Urs, J. Reermann, E. Yarar, A. Piorra, C. Kirchhof, E. Lage, M. Höft, G. U. Schmidt, *J. Mater. Res.* **2017**, *32*, 1009.

[53] J. Reermann, P. Durdaut, S. Salzer, T. Demming, A. Piorra, E. Quandt, N. Frey, M. Höft, G. Schmidt, *Measurement* **2018**, *116*, 230.

[54] S. Salzer, V. Röbisch, M. Klug, P. Durdaut, J. McCord, D. Meyners, J. Reermann, M. Höft, R. Knöchel, *IEEE Sens. J.* **2018**, *18*, 596.

[55] A. Kittmann, P. Durdaut, S. Zabel, J. Reermann, J. Schmalz, B. Spetzler, D. Meyners, N. X. Sun, J. McCord, M. Gerken, *Sci. Rep.* **2018**, *8*, 278.

[56] S. Salzer, P. Durdaut, V. Röbisch, D. Meyners, E. Quandt, M. Höft, R. Knöchel, *IEEE Sens. J.* **2016**, *17*, 1373.

[57] R. C. Chaves, P. P. Freitas, B. Ocker, W. Maass, *Appl. Phys. Lett.* **2007**, *91*, 102504.

[58] R. C. Chaves, P. P. Freitas, B. Ocker, W. Maass, *J. Appl. Phys.* **2008**, *103*, 07E931.

[59] S. Cardoso, D. C. Leitao, L. Gameiro, F. Cardoso, R. Ferreira, E. Paz, P. P. Freitas, *Microsyst. Technol.* **2014**, *20*, 793.

[60] S. H. Liou, X. Yin, S. E. Russek, R. Heindl, F. C. S. Da Silva, J. Moreland, D. P. Pappas, L. Yuan, J. Shen, *IEEE Trans. Magn.* **2011**, *47*, 3740.

[61] C. Zheng, K. Zhu, S. C. de Freitas, J.-Y. Chang, J. E. Davies, P. Eames, P. P. Freitas, O. Kazakova, C. Kim, C.-W. Leung, *IEEE Trans. Magn.* **2019**.

[62] S. Zuo, H. Fan, K. Nazarpour, H. Heidari, in *2019 IEEE Int. Symp. Circuits System (ISCAS)*, IEEE, Sapporo, Japan **2019**, p. 1.

[63] T. McGuire, R. L. Potter, *IEEE Trans. Magn.* **1975**, *11*, 1018.

[64] L. Jogschies, D. Klaas, R. Kruppe, J. Rittinger, P. Taptimthong, A. Wienecke, L. Rissing, M. C. Wurz, *Sensors* **2015**, *15*, 28665.

[65] J. Amaral, S. Cardoso, P. P. Freitas, A. M. Sebastião, *J. Appl. Phys.* **2011**, *109*, 07B308.

[66] J. Amaral, J. Gaspar, V. Pinto, T. Costa, N. Sousa, S. Cardoso, P. Freitas, *Appl. Phys. A* **2013**, *111*, 407.

[67] T. Costa, M. S. Piedade, J. Germano, J. Amaral, P. P. Freitas, *IEEE Trans. Instrum. Meas.* **2014**, *63*, 1171.

[68] M.-D. Cubells-Beltrán, C. Reig, J. Madrenas, A. De Marcellis, J. Santos, S. Cardoso, P. P. Freitas, *Sensors* **2016**, *16*, 939.

[69] M. Pannetier, C. Fermon, G. Le Goff, J. Simola, E. Kerr, *Science* **2004**, *304*, 1648.

[70] M. Pannetier, C. Fermon, G. Legoff, J. Simola, E. Kerr, M. Welling, R. J. Wijngaarden, *IEEE Trans. Appl. Supercond.* **2005**, *15*, 892.

[71] M. Pannetier-Lecoeur, C. Fermon, H. Dyvorne, J. F. Jacquinot, H. Polovy, A. L. Walliang, *J. Magn. Magn. Mater.* **2010**, *322*, 1647.

[72] J. Valadeiro, M. Silva, S. Cardoso, M. Martins, J. Gaspar, P. P. Freitas, A. M. Sebastião, in *Sensors Application Symp. (SAS), 2017 IEEE*, IEEE, Glassboro, NJ, USA **2017**, pp. 1–6.

[73] M. Pannetier-Lecoeur, L. Parkkonen, N. Sergeeva-Chollet, H. Polovy, C. Fermon, C. Fowley, *Appl. Phys. Lett.* **2011**, *98*, 153705.

[74] I. Ennen, D. Kappe, T. Rempel, C. Glenske, A. Hütten, *Sensors* **2016**, *16*, 904.

[75] S. Cardoso, D. C. Leitao, T. M. Dias, J. Valadeiro, M. D. Silva, A. Chicharo, V. Silverio, J. Gaspar, P. P. Freitas, *J. Phys. D: Appl. Phys.* **2017**, *50*, 213001.

[76] Z. Yin, E. Bonizzoni, H. Heidari, *IEEE J.Electromagn. RF Microwaves Med. Biol.* **2018**, *2*, 179.

[77] V. D. Krishna, K. Wu, A. M. Perez, J.-P. Wang, *Front. Microbiol.* **2016**, *7*, 400.

[78] T. M. Dias, F. A. Cardoso, S. A. M. Martins, V. C. Martins, S. Cardoso, J. F. Gaspar, G. Monteiro, P. P. Freitas, *Anal. Methods* **2016**, *8*, 119.

[79] M.-D. Cubells-Beltrán, C. Reig, A. De Marcellis, E. Figueras, A. Yúfera, B. Zadov, E. Paperno, S. Cardoso, P. P. Freitas, *Microelectron. J.* **2014**, *45*, 702.

[80] L. Caruso, T. Wunderle, C. M. Lewis, J. Valadeiro, V. Trauchessec, J. T. Rosillo, J. P. Amaral, J. Ni, P. Jendritza, C. Fermon, *Neuron* **2017**, *95*, 1283.

[81] J.-G. J. Zhu, C. Park, *Mater. Today* **2006**, *9*, 36.

[82] M. Julliere, *Phys. Lett. A* **1975**, *54*, 225.

[83] S. Zuo, K. Nazarpour, H. Heidari, *IEEE Electron Device Lett.* **2018**, *39*, 1784.

[84] D. E. Heim, R. E. Fontana, C. Tsang, V. S. Speriosu, B. A. Gurney, M. L. Williams, *IEEE Trans. Magn.* **1994**, *30*, 316.

[85] S. H. Voldman, A. J. Wallash, R. B. Wilcox Jr., *Patent US 5559051A*, **1996**.

[86] D. A. Hall, R. S. Gaster, K. A. A. Makinwa, S. X. Wang, B. Murmann, *IEEE J. Solid-State Circuits* **2013**, *48*, 1290.

[87] P. Wiśniowski, J. M. Almeida, S. Cardoso, N. P. Barradas, P. P. Freitas, *J. Appl. Phys.* **2008**, *103*, 07A910.

[88] S. de Freitas, *PhD thesis*, Instituto Superior Técnico, Universidade Técnica de Lisboa **2001**.

[89] Y. Ji, J. Liu, C. Yang, *J. Phys. D: Appl. Phys.* **2017**, *50*, 025005.

[90] P. P. Freitas, S. Cardoso, R. Ferreira, V. C. Martins, A. Guedes, F. A. Cardoso, J. Loureiro, R. Macedo, R. C. Chaves, J. Amaral, *Spin World Sci.* **2011**, *1*, 71.

[91] J. Amaral, V. Pinto, T. Costa, J. Gaspar, R. Ferreira, E. Paz, S. Cardoso, P. P. Freitas, *IEEE Trans. Magn.* **2013**, *49*, 3512.

[92] J. Valadeiro, S. Cardoso, R. Macedo, A. Guedes, J. Gaspar, P. P. Freitas, *Micromachines* **2016**, *7*, 88.

[93] H.-M. Shen, L. Hu, X. Fu, *Sensors* **2018**, *18*, 148.

[94] F. A. Cardoso, T. Costa, J. Germano, S. Cardoso, J. Borme, J. Gaspar, J. R. Fernandes, M. S. Piedade, P. P. Freitas, *IEEE Trans. Magn.* **2012**, *48*, 3784.

[95] V. Nabaei, R. Chandrawati, H. Heidari, *Biosens. Bioelectron.* **2018**, *103*, 69.

[96] E. Paz, R. Ferreira, P. P. Freitas, *IEEE Trans. Magn.* **2016**, *52*, 1.

[97] S. Cardoso, L. Gameiro, D. C. Leitao, F. Cardoso, R. Ferreira, E. Paz, P. P. Freitas, in *Smart Sensors, Actuators, MEMS VI*, International Society For Optics and Photonics, Grenoble, France **2013**, p. 87631A.

[98] A. V Silva, D. C. Leitao, J. Valadeiro, J. Amaral, P. P. Freitas, S. Cardoso, *Eur. Phys. J.: Appl. Phys.* **2015**, *72*, 10601.

[99] D. C. Leitao, L. Gameiro, A. V Silva, S. Cardoso, P. P. Freitas, *IEEE Trans. Magn.* **2012**, *48*, 3847.

[100] J. M. Almeida, P. P. Freitas, *J. Appl. Phys.* **2009**, *105*, 07E722.

[101] A. Guedes, J. M. Almeida, S. Cardoso, R. Ferreira, P. P. Freitas, *IEEE Trans. Magn.* **2007**, *43*, 2376.

[102] M. Pannetier, C. Fermon, G. Le Goff, J. Simola, E. Kerr, *Science* **2004**, *3*, 1.

[103] J. G. Deak, Z. Zhou, W. Shen, *AIP Adv.* **2017**, *7*, 056676.

[104] S.-H. Liou, X. Yin, S. E. Russek, R. Heindl, F. C. S. Da Silva, J. Moreland, D. P. Pappas, L. Yuan, J. Shen, *IEEE Trans. Magn.* **2011**, *47*, 3740.

[105] C. Barraud, C. Deranlot, P. Seneor, R. Mattana, B. Dlubak, S. Fusil, K. Bouzehouane, D. Deneuve, F. Petroff, A. Fert, *Appl. Phys. Lett.* **2010**, *96*, 072502.

[106] L. M. Loong, W. Lee, X. Qiu, P. Yang, H. Kawai, M. Saeys, J. Ahn, H. Yang, *Adv. Mater.* **2016**, *28*, 4983.

[107] J.-Y. Chen, Y.-C. Lau, J. M. D. Coey, M. Li, J.-P. Wang, *Sci. Rep.* **2017**, *7*, 42001.

[108] S. Ota, M. Ono, H. Matsumoto, A. Ando, T. Sekitani, R. Kohno, S. Iguchi, T. Koyama, D. Chiba, *Appl. Phys. Express* **2019**, *12*, 053001.

[109] J. Gaspar, H. Fonseca, E. Paz, M. Costa, M. Martins, R. Ferreira, S. Cardoso, P. Freitas, in *IEEE Int. Magnetics Conf. (INTERMAG)*, Beijing, China **2015**, p. 1.

[110] M. D. Cubells-Beltrán, C. Reig, D. R. Muñoz, S. I. P. C. De Freitas, P. J. P. De Freitas, *IEEE Sens. J.* **2009**, *9*, 1756.

[111] R. Ferreira, E. Paz, P. P. Freitas, J. Ribeiro, J. Germano, L. Sousa, *IEEE Trans. Magn.* **2012**, *48*, 4107.

[112] J. Cao, P. P. Freitas, *J. Appl. Phys.* **2010**, *107*, 09E712.

[113] C. Guiducci, A. Schmid, F. K. Gürkaynak, Y. Leblebici, in *Proc. Conf. Design Automation Test in Europe*, ACM, New York **2008**, pp. 1328–1333.

[114] M. A. C. Garcia, O. Baffa, *Front. Physiol.* **2015**, *6*, 1.

[115] Z. Wang, M. Xu, X. Xu, Z. Zhou, *2016 IEEE Int. Conf. Mechatronics and Automation*, IEEE, Harbin, China **2016**, p. 2209.

[116] T. Masuda, H. Endo, T. Takeda, S. Koga, A. Nakamura, D. Cohen, E. Givler, *Nuovo Cim. D* **1983**, *21*, 642.